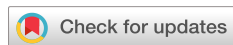


Linewidth narrowing in Raman lasers

R. L. Pahlavani   ; D. J. Spence  ; A. O. Sharp  ; R. P. Mildren 



APL Photonics 10, 076107 (2025)

<https://doi.org/10.1063/5.0271652>



Articles You May Be Interested In

Ultranarrow-linewidth stimulated Brillouin scattering with fundamental acoustic waves

APL Photonics (January 2025)

Phase locking and spectral linewidth of a two-mode terahertz quantum cascade laser

Appl. Phys. Lett. (July 2006)

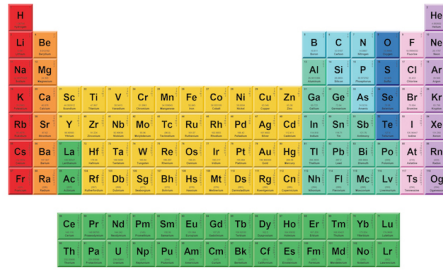
Power dependence of the linewidth enhancement term in semiconductor lasers

Appl. Phys. Lett. (June 1984)



THE MATERIALS SCIENCE MANUFACTURER®

Now Invent.™



American Elements
Opens a World of Possibilities

...Now Invent!

Linewidth narrowing in Raman lasers

Cite as: APL Photon. 10, 076107 (2025); doi: [10.1063/5.0271652](https://doi.org/10.1063/5.0271652)

Submitted: 19 March 2025 • Accepted: 19 June 2025 •

Published Online: 14 July 2025



View Online



Export Citation



CrossMark

R. L. Pahlavani,^{a)} D. J. Spence, A. O. Sharp, and R. P. Mildren

AFFILIATIONS

MQ Photonics Research Centre, Macquarie University, Sydney, Australia

^{a)}Author to whom correspondence should be addressed: richard.pahlavani@mq.edu.au

ABSTRACT

Raman lasers are well known for wavelength shifting and beam clean up, but less so for linewidth narrowing. Recent advances in design and material choice have enabled stable single frequency operation and the opportunity to investigate their narrow linewidth properties. Here, we use modeling and experiments to investigate linewidth and frequency noise as a function of pump noise. The model reveals that the picosecond-scale phonon dephasing time, typical of most Raman materials, suppresses pump frequency noise by factors up to 10^8 at Fourier frequencies up to 10^{11} Hz. To support the model, frequency noise spectra were measured for the input and output beams of a singly-resonant Raman laser operating at 1178 nm, revealing noise suppression by more than 10^4 at offset frequencies above 1 MHz. The results show that Raman lasers offer orders-of-magnitude greater linewidth-narrowing than Brillouin lasers, even for cavities of moderate Q factor. This makes them a promising route toward ultra-narrow linewidth lasers across the spectrum with adaptability to a wide range of pumps.

© 2025 Author(s). All article content, except where otherwise noted, is licensed under a Creative Commons Attribution (CC BY) license (<https://creativecommons.org/licenses/by/4.0/>). <https://doi.org/10.1063/5.0271652>

I. INTRODUCTION

Narrow-linewidth lasers are essential for a wide range of applications, including precision sensing, spectroscopy, and quantum science. In addition to the spectral width, the shape of the spectrum is an important factor depending on the application. For example, the power in the wings of a laser's line shape can introduce errors in the optical manipulation of qubits^{1,2} and impact precision in atomic clocks.^{3,4} In terms of laser frequency noise, Fourier components typically above 10^5 Hz arising from spontaneous emission into the lasing mode dictate the wing magnitude. Together with the Henry enhancement factor,⁵ these define the quantum limit, or Schawlow-Townes (ST) limit, which sets the lower bound for the effective linewidth achievable once technical noise such as cavity vibrations and length drift is mitigated.^{6,7} Minimization of the quantum noise is thus a critical aspect of narrow-linewidth laser design. In practice, the desired linewidth is engineered by addressing the key factors of the ST limit—through laser power, the use of high Q-factor cavities, and selecting gain media with low coupling between field amplitude and refractive index (low Henry factor). Lasers such as Ti:sapphire, fiber, and external-cavity diode lasers are examples that allow the Hz level linewidths needed in many of the most demanding coherent laser applications. Nevertheless, designing lasers that simultaneously satisfy the linewidth,

power, and wavelength requirements for a given application remains challenging.

Brillouin lasers offer a promising pathway to reduce the quantum noise properties of a given input laser. Acting essentially as add-on converters, they reduce input pump phase noise by taking advantage of the coupled acoustic phonon field, intrinsic to the stimulated Brillouin scattering interaction. Optical frequency noise is damped by the three-wave interaction when the Stokes amplitude lifetime in the cavity is longer than the phonon dephasing time, in which case pump phase perturbations are more strongly coupled to the phonon field than to the Stokes. The effect has been used to achieve^{8–11} reductions in Lorentzian linewidth by factors of 10^1 to 10^4 . With most Brillouin materials having phonon dephasing times in the nanosecond range, long cavity lifetimes (high cavity Q factors) are needed to achieve appreciable noise reductions. Nevertheless, some remarkably narrow Lorentzian linewidths have been achieved, including recent demonstrations at the tens of mHz level.^{9,12}

Stimulated Raman scattering shares a similar three-wave interaction, but with a range of other features, including phonon damping typically a thousand times larger, a large Stokes shift of the laser frequency, and phase matching conditions that enable forward as well as backward scattering. Raman lasers are well known as wavelength shifters and for beam clean-up, but their potential

for narrow-linewidth operation is largely unexplored. Here, we propose that lasers based on Raman gain are much more effective noise dampers than Brillouin and provide important advantages in design flexibility and wavelength range. Experimental progress in narrow-linewidth Raman lasers has enabled stable single longitudinal mode (SLM) operation despite the typically broad Raman gain bandwidth (10^1 – 10^3 GHz). Suppression of secondary modes has been achieved using narrow bandwidth Raman media,^{13,14} short cavities,^{15,16} and intracavity second harmonic generation.^{17,18} Linewidth narrowing factors up to 2000 have been observed.^{15,19–21} To date, however, the potential for Raman lasers as dampers of quantum noise has not been well articulated.

In this paper, we use the Raman three-wave coupled equations to model the frequency noise of the Stokes output as a function of pump noise and compare the results with the experiment. The model predicts linewidth narrowing factors of 10^8 and foreshadows sub-Hz Lorentzian linewidths even for near GHz linewidth pumps and cavities of modest Q factor, direct consequences of the large damping of the Raman phonons. The model is compared with the noise measurements for a drift-stabilized single-frequency diamond Raman laser operating with a pump with added phase noise using a phase modulator. The results show great potential for using the Raman interaction to diversify low-noise lasers and expand their range of power and frequency.

II. MODEL

The model considers a laser using a Raman gain medium of length L , segmented into N elements, in a cavity resonant for the Stokes, as depicted in Fig. 1. The input pump field contains a specified frequency noise spectrum and makes a double pass of the Raman medium by reflection from the output coupler (OC), as per the experimental conditions investigated below.

The model solves for the Stokes field E_s using the coupled three-wave equations,

$$\begin{aligned}\delta_t E_p &= i \frac{v_p g}{2\eta} E_s B, \\ \delta_t E_s &= i \frac{v_s g}{2} E_p B^*, \\ \delta_t B &= \frac{1}{T_2} (i E_p E_s^* - B),\end{aligned}\quad (1)$$

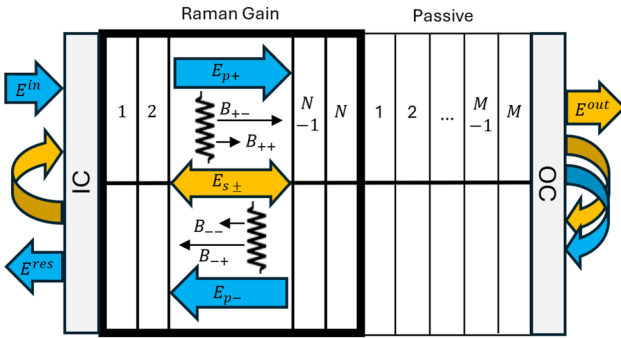


FIG. 1. Model structure with superimposed forward (upper) and backward (lower) pump propagation. The black arrows indicate the phonon field k -vectors for forward-scatter and backward-scatter for the first and second passes of the pump.

where B is proportional to the phonon field amplitude, $E_{s,p} = \sqrt{I_{s,p}}$ are the intracavity Stokes and pump field amplitudes, respectively, with I being the intensity, $*$ represents the complex conjugate, g is the Raman gain coefficient, $\eta = \lambda_s/\lambda_p$ is the quantum efficiency, δ_t is the temporal partial derivative, $v_{p,s} = c/n_{p,s}$ is the phase velocity of the wave in the material of refractive index $n_{p,s}$, and T_2 is the phonon dephasing time. Differentiation for each field is calculated and implemented for an interaction time $dt = L n_p / (Nc)$ before the fields are propagated through the cavity. The cavity optical path length was made variable to match the experiment by introducing M passive elements between the gain medium and OC (Fig. 1). To implement dispersion, the fields are displaced by one cell after the appropriate number of time steps.

Since both forward and backward scatter occur with equal strength for the Raman process, four distinct phonon fields, $B_{p\pm,s\pm}$, with different k -vectors emerge due to the bi-directional pump (Fig. 1). To track the various fields, the forward and backward directions are labeled + and –, respectively, with the first and second subscripts indicating pump and Stokes directionality. For example, B_{-+} refers to the phonon field that results from the interaction of a backward propagating pump with a forward propagating Stokes field. The phonon fields then have the form

$$\delta_t B_{\pm\pm} = \frac{dt}{T_2} (i E_{p\pm} (E_{s\pm})^* - B_{\pm\pm}). \quad (2)$$

The OC positioned at the $n = M^{\text{th}}$ cell is highly reflective (HR) for the pump and Stokes (with leakage $T = 1 - R$), and the input coupler (IC) at $n = 1$ is anti-reflective (AR) for the pump and HR for the Stokes, which enforce the boundary conditions,

$$\begin{aligned}&\text{Input Coupler} \\ &E_{p+}(n = 1, i) = E^{in}(i), \\ &E_{s+}(n = 1, i) = E_{s-}(n = 1, i - 1), \\ &E^{res}(i) = E_{p-}(n = 1, i), \\ &\text{Output Coupler} \\ &E_{p-}(n = M, i) = E_{p+}(n = M, i - 1), \\ &E_{s-}(n = M, i) = \sqrt{R} E_{s+}(n = M, i - 1), \\ &E^{out}(i) = \sqrt{1 - R} E_{s+}(n = M, i - 1),\end{aligned}\quad (3)$$

where $E^{in}(i)$ and $E^{out}(i)$ are the input pump and output Stokes fields for the i^{th} time step, respectively, and E^{res} is the residual pump field. Equation (1) is implemented at each cell before propagating the fields to the next cell.

The model can be used for any pump spectrum. In our case, the input pump field was constructed from the measured frequency noise spectrum (refer to Sec. IV) using

$$A_p(i) = \sqrt{f_s N_t} \mathcal{F}^{-1} \left[\sqrt{\frac{S_{vp}^{2S}(f)}{f^2}} \right], \quad (4)$$

where $S_{vp}(f)$ is the input frequency power spectral density (PSD) in units of Hz^2/Hz , \mathcal{F}^{-1} is the inverse Fourier transform, $A_p(i)$ is the

TABLE I. Model parameters corresponding to the experimental conditions. The model used $N = 200$ elements. $w_{p,s}$ is the $1/e^2$ spot radius, $n_{p,s}$ is the refractive index, and $\lambda_{p,s}$ is the wavelength for the pump and Stokes, respectively.

$w_{p,s}$	35 μm
g	10 cm/GW
Pump power	50 W
R	0.98
λ_p	1018 nm
λ_s	1178 nm
n_p	2.3755
n_s	2.3722
L	0.007 m
T_2	7 ps

normalized complex time series electric field amplitude, $2S$ refers to the 2-sided form of the PSD, f_s is the sampling frequency, N_t is the time series length, and f is the offset frequency. A random complex time series $P(i)$ for the model is generated by scaling $A_t(i)$ to the desired pump power.

The model was configured for our experimental parameters as summarized in Table I. For initial conditions, the Stokes field was seeded with a small amplitude (10^{-10} of its typical final value) with zero phase noise, and the acoustic field amplitude was zero. The model reached steady-state after time $T = 1.5 \mu\text{s}$. As shown in Fig. 2, the phase perturbations in the Stokes output are a small fraction of those on the input pump, varying by less than 0.25 rad over a period of 200 μs . The phase of the phonon field closely matches the pump, as expected due to the conservation of momentum. Field PSDs were calculated using Welch's estimation method with eight overlapping Blackman-Harris window segments. A comparison of the

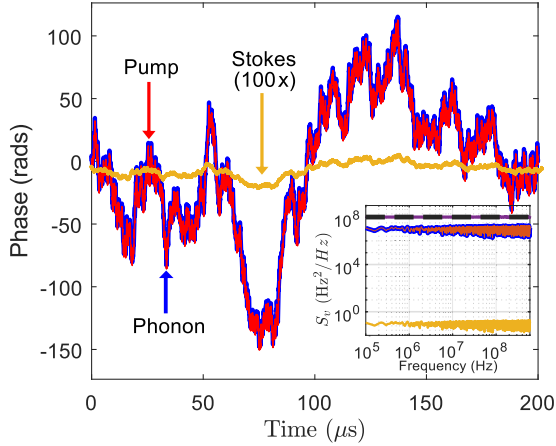


FIG. 2. Modeled phase evolution of the pump (red), Stokes (orange), and phonon (blue) fields. For the phonon field, the values for B_{+-} in the N^{th} cell are shown as a representative example. The Stokes vertical scale is expanded 100× to reveal the magnitude of the phase evolution. Insert: single-sided PSD of input pump, Stokes, and phonon fields. The noise reduction factor [$S_V(s)/S_V(p)$, purple line] is compared against the narrowing factor (K^2 , black dashed line) at each offset frequency. The phonon line in both plots has been emboldened to show its outline under the superimposed pump.

Stokes and pump PSDs (see insert of Fig. 2) shows noise reduction across the plotted frequency range, with a reduction of 1.05×10^8 in the frequency noise of the Stokes compared to the pump. The noise reduction factor closely agrees with the K^2 narrowing factor published for narrowing in a Brillouin system with a non-resonant pump,²²

$$K^2 = \frac{\Delta\nu_s}{\Delta\nu_p} = \left(1 + \frac{\tau_c}{T_2}\right)^2, \quad (5)$$

where $\Delta\nu_s, \Delta\nu_p$ are the Stokes and pump intrinsic linewidths, respectively, and $\tau_c = -2Ln_s/(c \log(\sqrt{R}))$ is the cavity amplitude lifetime. The model, therefore, confirms the large noise reduction capabilities of the Raman process and the generality of Eq. (5) for estimating the narrowing factor for Raman as well as Brillouin lasers for this type of configuration.

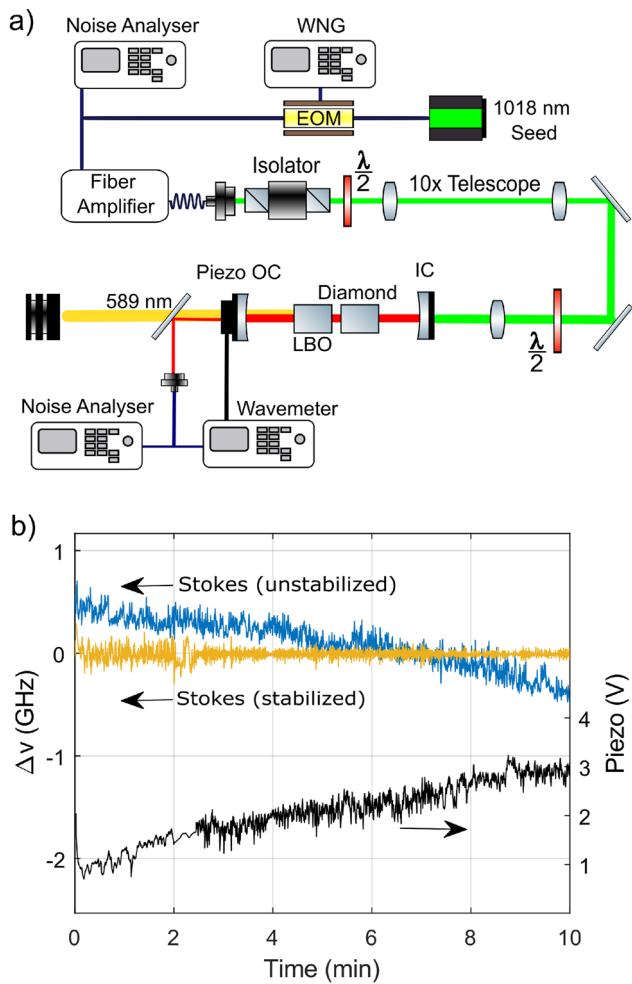


FIG. 3. (a) Laser setup schematic showing critical components. WNG: white noise generator, OC: output coupler, IC: input coupler, EOM: electro-optic modulator, LBO: lithium triborate, and $\lambda/2$: half-wave-plate. (b) Stokes frequency drift with (orange) and without (blue) feedback. For the feedback case, the piezo voltage is included to indicate the drift compensation.

III. EXPERIMENT

To support the model, a Raman laser using diamond as the gain medium was constructed, and the input and output frequency noise was measured using commercial linewidth analyzers. As shown in Fig. 3(a), a $2 \times 2 \times 7 \text{ mm}^3$ CVD-grown single-crystal diamond (low birefringence “Raman” grade, Element Six) was placed in a standing wave cavity of length $96 \pm 1 \text{ mm}$ [free-spectral-range (FSR) = 1.35 GHz] with mirrors of radius of curvature of 38 and 50 mm for the IC and OC, respectively. A lithium triborate crystal ($4 \times 4 \times 7 \text{ mm}^3$) was added to the cavity to enhance the stability of the single-longitudinal mode.^{17,23} For pump, Stokes, and second harmonic, respectively, the IC had coatings of HT, HR, and 10%R, and the OC had HR, 99%R, and 50%R.

The laser was pumped using a temperature stabilized 1018 nm seed laser (Moglabs CEL) that had phase noise added using an electro-optic modulator²⁴ driven by a white-noise generator with 1.5 GHz bandwidth. The broadened linewidth was also used to mitigate stimulated Brillouin scattering in the Yb fiber amplifier (Precilasers) used to generate input powers up to 50 W.

The small cavity FSR relative to the 45 GHz Raman gain bandwidth poses a challenge for stable mode-hop-free operation.²⁵ To address this, several measures were undertaken to increase the durations of mode-hop-free operation and to allow for reliable frequency noise measurement, in addition to the LBO crystal added to the cavity. These included a compact footprint for the pump beam delivery and laser cavity, a vibration-damped platform for mounting the cavity and pump transfer optics (Thorlabs B1224F 12" × 24" NEXUS), vibration-resistant mounts for cavity components (e.g., Newport 9081-M Five-Axis Alignment for diamond), and passive cooling of the diamond to eliminate coolant flow-induced vibrations. To compensate for thermal drift, the cavity length was stabilized via piezo-actuation of the OC (Thorlabs NFL5DP20) using the PID output of a wavemeter (HighFinesse WS6-200) monitoring the Stokes wavelength. The low wavemeter sample rate (500 Hz) and the considerable mass of the OC (>150 g) restricted the overall feedback bandwidth to less than a few hundred hertz.

IV. RESULTS

The laser threshold was 26 W and generated up to 5 W of second harmonic output from the OC at a pump power of 53 W. Note that the cavity was designed for stability rather than efficiency; hence, the output powers are lower than comparable devices in Refs. 23 and 26. Without thermal drift compensation, the laser operated mode-hop-free for over 10 min [Fig. 3(b)]. The prolonged mode-hop-free duration is attributed to the reduction of vibrations and increase in pump pointing stability through the mounting mechanisms discussed above. The wavelength increased during the observation period, attributed to the heating of the cavity components, eventually leading to a mode hop. Engaging wavemeter feedback mitigated the thermal drift, maintaining the Stokes predominantly within a 100 MHz band over a 15 min period, which was sufficiently long for the frequency noise measurements.

To measure the Raman laser frequency noise spectrum and linewidth, a 1 kHz resolution analyzer (HighFinesse LWA-10k NIR; 1064–1625 nm) was used. A second analyzer (OEwaves OE-4000;

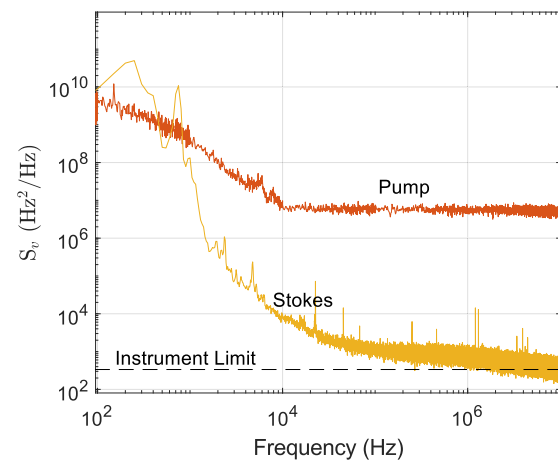


FIG. 4. Single-sided PSD measurements of pump seed and Stokes showing large noise narrowing occurring at high frequencies. The instrument resolution limit for the Stokes is indicated.

3 Hz resolution; 980–1080 nm) was used for the pump. Pump characterization was performed for the seed, as the noise introduced from the fiber amplifier is expected to be negligible compared to the induced EOM linewidth broadening.²⁷

A comparison of the Stokes and pump PSDs (Fig. 4) shows that the frequency noise at offset frequencies above 10 kHz is strongly damped in the Raman laser. The overall shape of the spectrum includes substantial $1/f^\alpha$ noise at low frequencies that decreases to an almost flat spectrum at offset frequencies above 50 kHz. There is a notable peak at 750 Hz, which may be related to a mechanical resonance with the oscillator cavity. At the maximum measured offset frequency of 10 MHz, the noise decreases from $5.1 \times 10^6 \text{ Hz}^2/\text{Hz}$ for the pump to $320 \text{ Hz}^2/\text{Hz}$ for the Stokes, which corresponds to a noise reduction factor of more than 1.6×10^4 . The Lorentzian linewidth of the Raman laser, calculated using πS_o , where S_o is the PSD white noise component, is $1.0 \pm 0.1 \text{ kHz}$. Since the frequency noise at higher offsets hits the resolution limit of the instrument, the observed noise reduction is expected to be a lower bound on the actual noise reduction. The Stokes frequency noise increases rapidly at offsets below 50 kHz, which is expected since no stabilization was used apart from drift compensation, and therefore the integrated linewidth remains broad (7.6 MHz for an integration time of 20 ms).

V. DISCUSSION

The 16 000-fold reduction in high-frequency noise is consistent with the strong phonon noise damping expected in Raman lasers. Although the reduction is not as large as that predicted by the model, we expect this discrepancy to diminish with improved measurement sensitivity. The model suggests that the reduction may be as large as 1×10^8 , which for our present pump would correspond to a Lorentzian linewidth of hundreds of millihertz. Such noise reduction and linewidth narrowing are obtained even for a cavity $Q = 5.8 \times 10^7$, which is modest compared to that of many low noise lasers, such as those based on whispering gallery mode cavities.

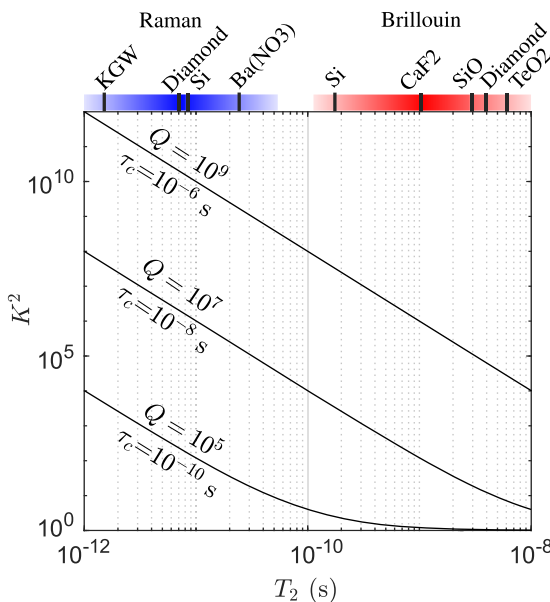


FIG. 5. Linewidth narrowing factors [K^2 ; Eq. (5)] as a function of T_2 for various materials and regimes (Brillouin²⁸ and Raman²⁹) for three cavity amplitude lifetimes and equivalent cavity Q factors (calculated with $\lambda = 1 \mu\text{m}$).

Compared to Brillouin lasers, an equivalent Raman system is expected to suppress noise by a further $K_R^2/K_B^2 \sim 10^6$, owing to their typically thousand times shorter T_2 times. Figure 5 shows the narrowing factors achievable for a range of typical Q factors as a function of T_2 , comparing Raman and Brillouin lasers. Even for cavities of modest Q (10^6 to 10^7), the narrowing factors are above 10^5 for most Raman materials, whereas very little narrowing would be obtained for an equivalent laser using the Brillouin interaction. These large suppression factors and pump laser flexibilities open up new design freedoms for expanding the wavelength range and increasing power and make Raman lasers promising for applications requiring ultra-narrow linewidths. Clock lasers, for example, typically require sub-kHz-level linewidths depending on the level of precision needed. The sub-kHz intrinsic linewidth of the current device is already in the regime required for this application and others that require such levels of frequency precision.

The model further suggests that the noise suppression occurs up to the gain bandwidth $(\pi T_2)^{-1}$ in offset frequency (roughly 50 GHz in diamond), and therefore pump power within this bandwidth is efficiently coupled into the narrow-linewidth output.

Linewidth narrowing via phonon damping is ultimately limited by the ST limit for the Raman laser, which contains a term involving the Boltzmann population of the phonon.⁸ Due to the higher phonon frequency, and therefore lower thermal phonon density, the ST limit is narrower than an equivalent laser based on stimulated Brillouin scattering.^{8,16} In the case of diamond Raman lasers, output powers (10s W) are typically much higher than Brillouin systems (sub-watt). As a result, the estimated ST limit of the present laser is calculated to be on the order of 1 μHz , which is well below the experimental and modeled values. An ST-limited linewidth may be

achieved by using a narrow pump linewidth of up to 10s Hz. Future work using monolithic Raman cavities^{30,31} to reduce low frequency noise provides a pathway to ultra-narrow effective linewidth systems with multi-watt output powers.

VI. CONCLUSION

Numerical modeling of the Raman interaction shows that the heavily damped phonons provide a pathway to radically lower quantum noise, with predicted suppression factors typically more than 10^5 and 10^6 times higher than Brillouin lasers. Experimentally, a noise reduction of 1.6×10^4 at 1 MHz offset, resolution limited, was obtained using diamond as the Raman material. Raman noise suppression is promising for creating a new generation of ultra-narrow-linewidth lasers, using only modest Q-cavities, and operating at wavelengths across the spectrum.

ACKNOWLEDGMENTS

This work was sponsored by the Australian Research Council (Grant No. LP200301594) and the U.S. Air Force Office of Scientific Research (Grant No. FA2386-21-1-4030). We also acknowledge EOS Space Systems for funding and scholarship (RLP) support.

AUTHOR DECLARATIONS

Conflict of Interest

The authors have no conflicts to disclose.

Author Contributions

R. L. Pahlavani: Data curation (equal); Formal analysis (equal); Methodology (equal); Writing – original draft (equal); Writing – review & editing (equal). **D. J. Spence:** Conceptualization (supporting); Formal analysis (equal); Methodology (equal); Supervision (supporting); Writing – review & editing (supporting). **A. O. Sharp:** Data curation (supporting); Writing – review & editing (supporting). **R. P. Mildren:** Conceptualization (equal); Formal analysis (equal); Funding acquisition (equal); Methodology (equal); Supervision (equal); Writing – review & editing (equal).

DATA AVAILABILITY

The data that support the findings of this study are available from the corresponding author upon reasonable request.

REFERENCES

- M. L. Day, P. J. Low, B. White, R. Islam, and C. Senko, “Limits on atomic qubit control from laser noise,” *npj Quantum Inf.* **8**, 72 (2022).
- H. Nakav, R. Finkelstein, L. Peleg, N. Akerman, and R. Ozeri, “Effect of fast noise on the fidelity of trapped-ion quantum gates,” *Phys. Rev. A* **107**, 042622 (2023).
- A. Quessada, R. P. Kovacich, I. Courtillot, A. Clairon, G. Santarelli, and P. Lemonde, “The Dick effect for an optical frequency standard,” *J. Opt. B: Quantum Semiclassical Opt.* **5**, S150 (2003).
- T. Nazarov, H. Schnatz, B. Lipphardt, F. Riehle, U. Sterr, and C. Lisdat, “Influence of high-frequency laser frequency noise on the stability of an optical

- clock,” in *2007 IEEE International Frequency Control Symposium Joint with the 21st European Frequency and Time Forum* (IEEE, 2007), pp. 111–114.
- ⁵C. Henry, “Theory of the linewidth of semiconductor lasers,” *IEEE J. Quantum Electron.* **18**, 259–264 (1982).
- ⁶A. L. Schawlow and C. H. Townes, “Infrared and optical masers,” *Phys. Rev.* **112**, 1940 (1958).
- ⁷T. J. Baker, S. N. Saadatmand, D. W. Berry, and H. M. Wiseman, “The Heisenberg limit for laser coherence,” *Nat. Phys.* **17**, 179–183 (2021).
- ⁸J. Li, H. Lee, T. Chen, and K. J. Vahala, “Characterization of a high coherence, Brillouin microcavity laser on silicon,” *Opt. Express* **20**, 20170–20180 (2012).
- ⁹K. Liu, J. Wang, N. Chauhan, M. W. Harrington, K. D. Nelson, and D. J. Blumenthal, “Integrated photonic molecule Brillouin laser with a high-power sub-100-mHz fundamental linewidth,” *Opt. Lett.* **49**, 45–48 (2023).
- ¹⁰D. Jin, Z. Bai, Z. Zhao, Y. Chen, W. Fan, Y. Wang, R. P. Mildren, and Z. Lü, “Linewidth narrowing in free-space-running diamond Brillouin lasers,” *High Power Laser Sci. Eng.* **11**, e47 (2023).
- ¹¹Z. Bai, H. Yuan, Z. Liu, P. Xu, Q. Gao, R. J. Williams, O. Kitzler, R. P. Mildren, Y. Wang, and Z. Lu, “Stimulated Brillouin scattering materials, experimental design and applications: A review,” *Opt. Mater.* **75**, 626–645 (2018).
- ¹²M. Alouini, G. Danion, and M. Vallet, “Self-linewidth-narrowing photonic oscillator,” *Opt. Express* **33**, 1021–1033 (2025).
- ¹³L. S. Meng, P. A. Roos, and J. L. Carlsten, “Continuous-wave rotational Raman laser in H₂,” *Opt. Lett.* **27**, 1226–1228 (2002).
- ¹⁴C. Y. Lee, C. C. Chang, P. H. Tuan, C. Y. Cho, K.-F. Huang, and Y.-F. Chen, “Cryogenically monolithic self-Raman lasers: Observation of single-longitudinal-mode operation,” *Opt. Lett.* **40**, 1996–1999 (2015).
- ¹⁵E. Granados, G. Stoikos, D. T. Echarri, K. Chrysaliidis, V. N. Fedossev, C. Granados, V. Leask, B. A. Marsh, and R. P. Mildren, “Tunable spectral squeezers based on monolithically integrated diamond Raman resonators,” *Appl. Phys. Lett.* **120**, 151101 (2022).
- ¹⁶K. Liu, S. Yao, Y. Ding, Z. Wang, Y. Guo, J. Yan, J. Wang, C. Yang, and C. Bao, “Fundamental linewidth of an AlN microcavity Raman laser,” *Opt. Lett.* **47**, 4295–4298 (2022).
- ¹⁷X. Yang, O. Kitzler, D. J. Spence, R. J. Williams, Z. Bai, S. Sarang, L. Zhang, Y. Feng, and R. P. Mildren, “Single-frequency 620 nm diamond laser at high power, stabilized via harmonic self-suppression and spatial-hole-burning-free gain,” *Opt. Lett.* **44**, 839–842 (2019).
- ¹⁸K. I. Martin, W. A. Clarkson, and D. C. Hanna, “Self-suppression of axial mode hopping by intracavity second-harmonic generation,” *Opt. Lett.* **22**, 375–377 (1997).
- ¹⁹Y. Cai, F. Gao, H. Chen, X. Yang, Z. Bai, Y. Qi, Y. Wang, Z. Lu, and J. Ding, “Continuous-wave diamond laser with a tunable wavelength in orange-red wavelength band,” *Opt. Commun.* **528**, 128985 (2023).
- ²⁰Y. Sun, X. Yang, M. Li, X. Zeng, H. Jiang, and Y. Feng, “Diamond guide star laser pulsed at a Larmor frequency,” *Opt. Express* **32**, 46345–46352 (2024).
- ²¹C. Shen, X. Cai, X. Su, T. Zheng, J. Liu, Y. Chen, Y. Jia, D. Liu, and J. Guo, “Wavelength-tunable narrow-linewidth gaseous Raman laser,” *Appl. Opt.* **60**, 5465–5470 (2021).
- ²²A. Debut, S. Randoux, and J. Zemmouri, “Linewidth narrowing in Brillouin lasers: Theoretical analysis,” *Phys. Rev. A* **62**, 023803 (2000).
- ²³X. Yang, O. Kitzler, D. J. Spence, Z. Bai, Y. Feng, and R. P. Mildren, “Diamond sodium guide star laser,” *Opt. Lett.* **45**, 1898–1901 (2020).
- ²⁴G. N. West, W. Loh, D. Kharas, and R. J. Ram, “Impact of laser frequency noise on high-extinction optical modulation,” *Opt. Express* **28**, 39606–39617 (2020).
- ²⁵O. Lux, S. Sarang, O. Kitzler, D. J. Spence, and R. P. Mildren, “Intrinsically stable high-power single longitudinal mode laser using spatial hole burning free gain,” *Optica* **3**, 876–881 (2016).
- ²⁶Y. Sun, M. Li, O. Kitzler, R. P. Mildren, Z. Bai, H. Zhang, J. Lu, Y. Feng, and X. Yang, “Stable high-efficiency continuous-wave diamond Raman laser at 1178 nm,” *Laser Phys. Lett.* **19**, 125001 (2022).
- ²⁷I. Ricciardi, S. Mosca, P. Maddaloni, L. Santamaria, M. De Rosa, and P. De Natale, “Phase noise analysis of a 10 Watt Yb-doped fibre amplifier seeded by a 1-Hz-linewidth laser,” *Opt. Express* **21**, 14618–14626 (2013).
- ²⁸Z. Bai, R. J. Williams, O. Kitzler, S. Sarang, D. J. Spence, Y. Wang, Z. Lu, and R. P. Mildren, “Diamond Brillouin laser in the visible,” *APL Photonics* **5**, 031301 (2020).
- ²⁹R. P. Mildren, A. Sabella, O. Kitzler, D. J. Spence, and A. M. McKay, “Diamond Raman laser design and performance,” in *Optical Engineering of Diamond* (Wiley, 2013), pp. 239–276.
- ³⁰W. Zhang, E. Kittlaus, A. Savchenkov, V. Iltchenko, L. Yi, S. B. Papp, and A. Matsko, “Monolithic optical resonator for ultrastable laser and photonic millimeter-wave synthesis,” *Commun. Phys.* **7**, 177 (2024).
- ³¹D. J. Little, R. L. Pahlavani, and R. P. Mildren, “Modulation depth and bandwidth analysis of planar thermo-optic diamond actuators,” *Opt. Express* **31**, 153–162 (2022).